Deep Resources Engineering 2 (2025) 100174

Contents lists available at ScienceDirect

Deep Resources Engineering

journal homepage: www.keaipublishing.com/en/journals/deepre/

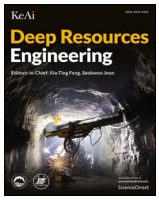

Full Length Article

Process system modelling of gas injection characteristics for underground CAES

LiGe Wang [a,b], Cunzhuang Lu [a,b], Shishu Zhang [c], Di Peng [d,e], Qingrong Xiong [f], Xizhong Chen [g], Hongling Ma [h], Zizheng Sun [a,b], Liping Li [a,b,*]

[a] School of Qilu Transportation, Shandong University, Jinan 250061, China
[b] State Key Laboratory of Intelligent Manufacturing of Advanced Construction Machinery, Jinan 250012, China
[c] Powerchina Chengdu Engineering Corporation Limited, Chengdu 610072, China
[d] Institute of Foundation Engineering, China Academy of Building Research, Beijing 100013, China
[e] State Key Laboratory of Building Safety and Environment, Beijing 100013, China
[f] School of Civil Engineering, Shandong University, Jinan 250061, China
[g] Department of Chemical Engineering, School of Chemistry and Chemical Engineering, Shanghai Jiao Tong University, Shanghai 200240, China
[h] State Key Laboratory of Geomechanics and Geotechnical Engineering, Institute of Rock and Soil Mechanics, Chinese Academy of Science, Wuhan 430071, China

ARTICLE INFO

Keywords:
Renewable energy
Compressed air energy storage (CAES)
Underground cavern
System integration
Process system modelling

ABSTRACT

Renewable energies including solar and wind are intermittent, causing difficulty in connection to conventional power grids due to instability of output duty. Compressed air energy storage (CAES) in underground caverns has been considered a potential large-scale energy storage technology. In order to explore the gas injection characteristic of underground cavern, a detailed thermodynamic model of the system is established in the process modelling software gPROMS. The four subsystem models, i.e. the compressor, heat exchanger, underground cavern storage and expander, are connected with inlet-outlet equilibrium of flow rate/pressure/temperature to form an integrated CAES system model in gPROMS. The maximum air pressure and temperature in the cavern are focused to interrogate the critical condition of the cavern during the injection process. When analyzing the mass flow rate-pressure ratio relationship, it's found that under specified operating conditions, an increase in mass flow rate can lead to a higher pressure ratio. Compression power demand also escalates significantly with increasing mass flow rates, underscoring the system's energy-intensive nature. Additionally, the cooler outlet energy rate progressively decreases, becoming increasingly negative as the mass flow rate increases. These insights offer critical theoretical foundations for optimizing practical efficiency of CAES.

1. Introduction

The accelerated development of renewable energy (wind and solar energy) has emerged as a critical pathway to address the global energy crisis and achieving carbon neutrality [1,2]. According to International Energy Agency projections, which renewable energy anticipated to comprise over 85 % of total energy production within the next three decades [3]. However, these renewable energy sources have the features of stochasticity, volatility and intermittence. These inherent defects may seriously damage the normal operation of the conventional power grid [4,5]. Therefore, developing large-scale energy storage technology is both necessary and effective for harnessing renewable energy [6,7]. Currently, large-scale energy storage technologies can be classified as mechanical, electrochemical, electromagnetic energy storage, and so on [8–12]. Among them, mechanical and electrochemical energy storage are more widely adopted. Pumped hydro energy storage (PHES) and compressed air energy storage (CAES) have emerged as predominant technological pathways owing to merits (energy density and storage capacity) [13]. In contrast, CAES is the most suitable large-scale energy technology by virtue of flexibility [14].

The principle and configuration of CAES are illustrated in Fig. 1. CAES utilizes surplus electricity to drive multistage compressors. The pressurized air is stored in geological reservoirs (salt caverns, aquifers and hard rock caverns) or pressure vessels. When electricity demand peaks stored air is released to drive the expands to generate electricity [15–18]. At present, two CAES power plants (Huntorf and McIntosh)

* Corresponding author at: School of Qilu Transportation, Shandong University, Jinan 250061, China.
E-mail address: yuliyangfan@163.com (L. Li).

https://doi.org/10.1016/j.deepre.2025.100174
Received 12 November 2024; Received in revised form 27 March 2025; Accepted 27 March 2025
Available online 5 April 2025

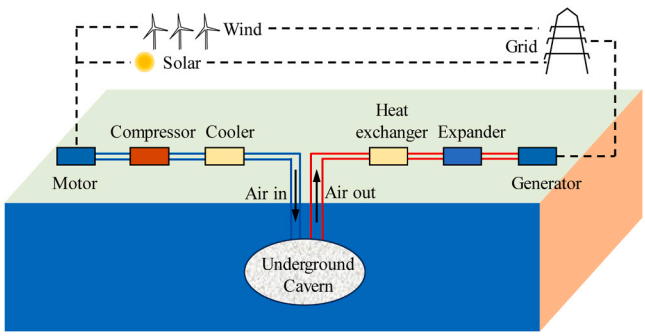

Fig. 1. Schematic diagram of a CAES system (Adapted from [18]).

have been put into commercial operation abroad. Both CAES power plants use underground salt caverns to store gas, and both use refueling CAES technology, which requires external fossil fuels and has not yet transitioned away from non-renewable energy sources [19–21]. In recent years, advanced CAES systems have been developed, including advanced adiabatic(AA) CAES [22], isothermal CAES [23], and liquid air energy storage [24].

Many attempts have been made towards the operational behavior for CAES systems. Hossein et al. [25] a decentralized CAES configuration with compressors co-located near thermal demand zones, demonstrating enhanced economic viability through waste heat monetization in Alberta's energy market. Lv et al. [26] optimized the relevant parameters affecting the system performance of the CAES based on the established thermodynamic model. Sciacovelli et al. [27] analyzed the transient characteristics of the compression/expansion phase, heat storage and air temperature in the reservoir and obtained the relationship between the equipment and system efficiency. He et al. [28] proposed the thermodynamic model with variable pressure ratio CAES and analyzed the output work of the compressor/expander, and the charging and discharging efficiency of the CAES. Jin et al. [29] developed a dynamic model for a hybrid CAES-wind turbine system, achieving 38 % power fluctuation mitigation and 3-hour operational stability enhancement validated through transient simulation. Arabkoohsar et al. [30] developed a thermodynamic model for the AA-CAES system based on the actual status of key components. It is shown that the system's cycling efficiency differed significantly under varying operating conditions.

However, few studies consider the integration process of CAES. Furthermore, the underground cavern falls short of the critical information of air conditions such as air temperature and pressure due to the disconnection between the over&under-ground subsystems. Therefore, a process system model of CAES allows for the simulation of dynamic system interactions and optimization of performance, providing a distinct advantage in system design and analysis. In this paper, a CAES model comprising sub-models of compressor, heat exchanger, underground cavern storage and expander is integrated, and all of these are implemented in gPROMS, an advanced process system modelling platform.

2. Mathematical theoretical models

The key components of CAES system includes but are not limited to generator, compressors, heat exchangers, underground cavern storage and expanders. The CAES system model established in this paper can accurately simulate the actual operation process, which provides a theoretical basis for the study of the dynamic characteristics and operation characteristics of large-capacity CAES. There are some key assumptions for the modelled as follows:

(1) Compressed air is considered to be ideal gas.
(2) The pipeline pressure drop is neglected.
(3) The ambient pressure and temperature remain constant.
(4) The heat transfer between the air inside the compressor and the external environment is neglected.
(5) The compressor is always operating in rated condition.
(6) The compression process is regarded as isentropic compression.

2.1. Compressor model

The compressor, serving as the core component of a CAES system, pressurizes air by converting mechanical energy into internal energy. The centrifugal compressor model can be used to represent multiple consecutive compression stages.

According to the principle of isentropic process, the temperature and pressure of an ideal gas are satisfied in isentropic compression:

$$\frac{T_{2s}}{T_1} = \left(\frac{p_2}{p_1}\right)^{\frac{\gamma-1}{\gamma}} \tag{1}$$

where $T_{2s}$is the isentropic outlet temperature, T_1 is inlet temperature, p_2 is outlet pressure, p_1 is inlet pressure, γ is the specific heat ratio, $\gamma = c_p/c_v$, $c_p$is the constant pressure specific heat capacity and c_v is the constant volume specific heat capacity.

The actual compression process has irreversible losses that need to be corrected with isentropic efficiency. Introducing isentropic efficiency η_{is}, the isentropic efficiency of the compressor is defined as:

$$\eta_{\text{is}} = \frac{T_{2s} - T_1}{T_2 - T_1} \tag{2}$$

where T_2 is the outlet temperature, this gives the actual outlet temperature:

$$T_2 = T_1 + \frac{T_{2s} - T_1}{\eta_{\text{is}}} \tag{3}$$

Substitute $T_{2s} = T_1\left(\frac{p_2}{p_1}\right)^{\frac{\gamma-1}{\gamma}}$ into the above equation:

$$T_2 = T_1 + \frac{T_1\left(\frac{p_2}{p_1}\right)^{\frac{\gamma-1}{\gamma}} - T_1}{\eta_{\text{is}}} \tag{4}$$

The simplification can be obtained:

$$T_2 = T_1\left[1 + \frac{1}{\eta_{\text{is}}}\left(\left(\frac{p_2}{p_1}\right)^{\frac{\gamma-1}{\gamma}} - 1\right)\right] \tag{5}$$

The compression power P_c can be expressed as:

$$P_{\text{c}} = \dot{m}\frac{1}{\eta_{\text{is}}}\frac{\gamma}{\gamma-1}R_m T_1\left[\left(\frac{p_2}{p_1}\right)^{\frac{\gamma-1}{\gamma}} - 1\right] \tag{6}$$

where $\dot{m}$ is the mass flow rate of air and R_m is the air constant.

2.2. Heat exchanger model

Heat exchangers in CAES systems perform critical interstage thermal regulation by transferring compression-generated heat to thermal storage media. In this paper, the heat exchanger effectiveness ε can be expressed as [29]:

$$\varepsilon = \frac{c_{p,c}\dot{m}_c\left(T_{2,c} - T_{1,c}\right)}{\left(c_p\dot{m}\right)_{\min}\left(T_{1,c} - T_{1,h}\right)} = \frac{c_{p,h}\dot{m}_h\left(T_{2,h} - T_{1,h}\right)}{\left(c_p\dot{m}\right)_{\min}\left(T_{1,c} - T_{1,h}\right)} \tag{7}$$

where c_p is the constant pressure specific heat capacity, the subscript c is cold fluid (water), and h is hot fluid (air). $\dot{m}_c$ is the cold fluid (water)

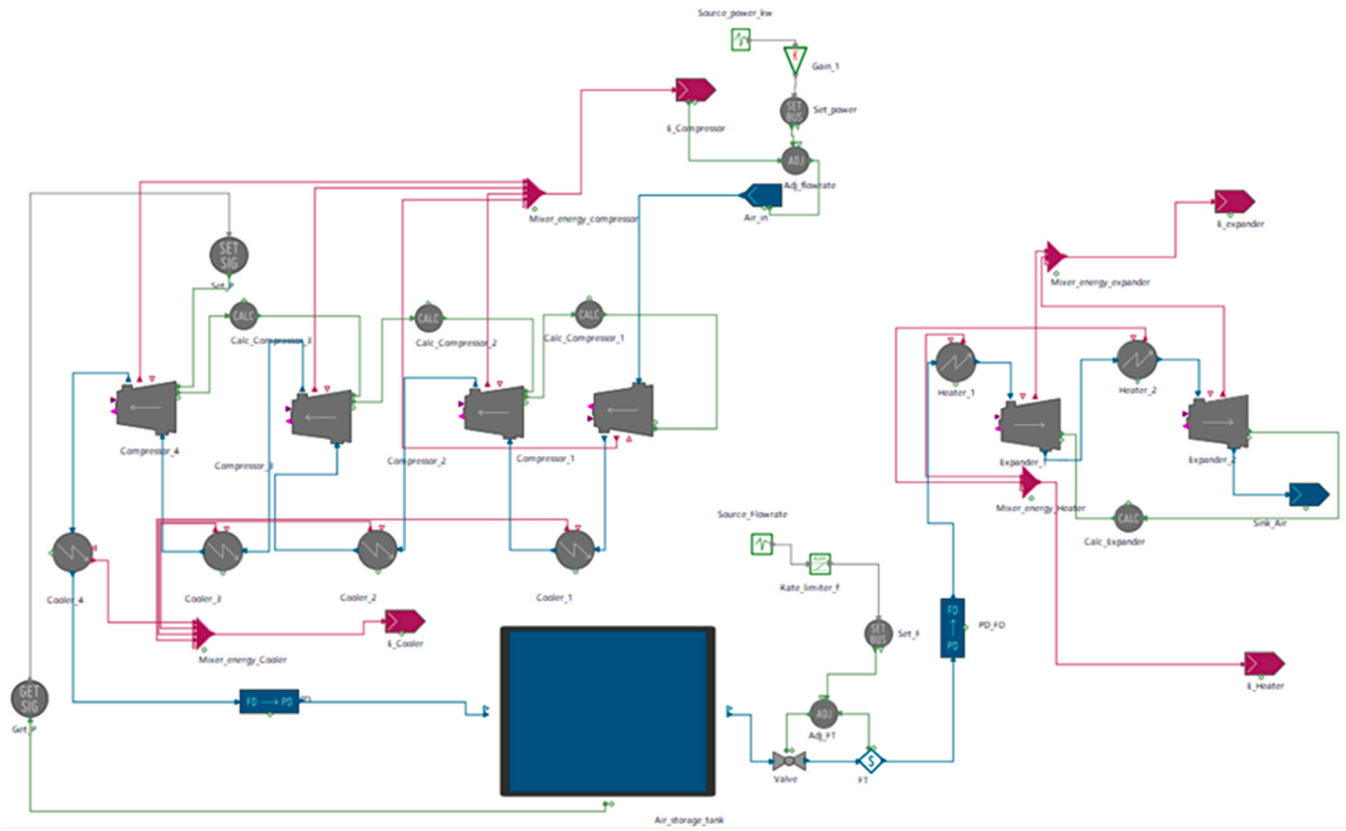

Fig. 2. Modelling flowsheet of the CAES system.

mass flow, $T_{1,c}$ is the expander inlet air temperature, $T_{2,c}$ is the expander outlet air temperature, $(c_p\dot{m})_{\min}$indicates the minimum between$(c_{p,c}\dot{m}_c)$ and $(c_{p,h}\dot{m}_h)$, $\dot{m}_h$ is the hot fluid (air) mass flow, $T_{1,h}$ is the hot fluid (air) inlet temperature, $T_{2,c}$ is the hot fluid (air) outlet temperature.

The above equation can be further simplified, and the outlet temperature T_2 can be expressed as [29]:

$$T_2 = (1-\varepsilon)T_1 + \varepsilon T_{1,c} \tag{8}$$

It is noteworthy that pressure drop occurs when air passes through a heat exchanger. In this paper, this pressure drop Δp can be expressed as [29]:

$$\frac{\Delta p}{p_1} = \frac{0.0083\varepsilon}{1-\varepsilon} \tag{9}$$

2.3. Expander model

The operating mechanism of the expander can be understood as an inverse process of the compressor. It is mathematically modeled using the compressor modeling approach. For a single stage this relationship is:

$$T_2 = T_1\left[1-\eta_{\text{is}}\left(1-\left(\frac{p_{1t}}{p_{2t}}\right)^{\frac{1-\gamma}{\gamma}}\right)\right] \tag{10}$$

$$P_t = \dot{m}\eta_{\text{is}}\frac{\gamma}{\gamma-1}R_m T_1\left(1-\left(\frac{p_{1t}}{p_{2t}}\right)^{\frac{1-\gamma}{\gamma}}\right) \tag{11}$$

where p_{2t} is expander outlet pressure, p_{1t} is expander inlet pressure, $\frac{p_{1t}}{p_{2t}}$is the expansion ratio, P_t is the expander output power.

It is noteworthy that this paper doesn't take the expander module into account in the compressor stage. The current study focuses on the injection characterisation, whereas the expander only plays a major role in the venting process. However, it is necessary to retain the expander in the current model in order to ensure the integrity of the process system, which will be outlined in more detail in the next article. The expander's role in energy recovery and system efficiency will be addressed in a subsequent study, where key parameters such as isentropic efficiency and thermal effects during expansion will be examined to optimize overall system performance.

2.4. Underground cavern storage model

The thermodynamic and mass transfer interdependencies between the storage cavern and compression/expansion subsystems fundamentally dictate CAES system performance. Typically, energy storage in CAES systems is situated within geological formations, such as bedded salt caverns or salt domes [31], aquifers [32], depleted gas reservoirs [33], or lined rock caverns [34]. The integrity and functionality of the gas storage modules are essential, as they directly influence the reliability and efficiency of the entire system. As a key feature of the established model, it is universal for the underground cavern to be representative of various categories as abovementioned. This is due to the fact that gPROMS software offers general modeling capability for underground caverns. Nevertheless, the input parameters such as the cavern volume, surface area, density, heat transfer coefficient are varying with the cavern types. As such, gPROMS can distinguish different types of caverns in recognition of these dissimilarities such as thermodynamic and dynamic processes.

According to the ideal gas state equation, mass conservation equation and energy balance equation [29]:

$$p_{\text{cavern}}V = MRT \tag{12}$$

$$\frac{\mathrm{d}M}{\mathrm{d}t} = \dot{m}_{\text{in}} - \dot{m}_{\text{out}} \tag{13}$$

Table 1
Model symbol of CAES system.

Model symbol	Name	Feature
	Compressor	Air from the atmosphere is drawn in and compressed, thereby converting electrical energy into the internal energy of the air.
	Cooler	The heat generated will be transferred out, so that the temperature of the compressed air is reduced to a suitable range, reducing energy loss.
	Valve	The valve model simulates the flow of a fluid through a valve, and defines a flow-pressure relation.
	Heater	The heater model is used to increase the temperature of a material stream.
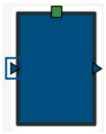	Underground cavern storage	The underground cavern storage model is used to model a vessel for the storage of gas.
	Expander	The high-pressure compressed air is released, creating a high-speed airflow that drives a expander to spin and generate electricity.
	Get signal from bus	The Get signal from bus model is used to select a variable from a unit equipment model or a stream analyser and obtain the value as a signal variable.
	Calc spec	The Calc spec model calculates the value of an output variable by performing a linear transformation of an input variable value.
	Mixer energy	The Mixer energy model is used to mix different energy inlet streams into a single outlet energy stream.
	Sink energy	The Sink energy model is the point where an energy stream leaves the flowsheet.
	gML Material flow-driven to Pressure-driven	The gML Material flow-driven to pressure-driven model transforms an upstream flow-driven section of a flowsheet into a pressure-driven downstream section.
	Source linear interpolated	The time profile of the output values is a linearly interpolated signal between a given set of points.
	Gain parameter	Multiply all values in the input variable vector by a fixed gain. The gain value is a parameter.
	Set signal to created bus	The Set signal to created bus model is used to select a variable from a gMLBus connection of which the variable type is specified and set the value of that variable based on a signal variable input. It can be used to interface from gMLSignal to gMLBus connections.

Table 1 (*continued*)

Model symbol	Name	Feature
	Adj spec	The Adj spec model can be used to trade-off specifications between different models.
	Rate limiter	When the rate of change of the input values is within given limits, the outlet values track the inlet values closely. When the rate of change of the inlet values exceed the limits, the rate of change of the outlet values is limited to the specified limits.
	Stream analyzer	The Stream analyzer model can be used to report a range of material stream properties or compositions and properties of individual phases present in the material stream.
	Source material	The Source material model is the point where a material stream enters the flowsheet.
	Sink material	The Sink material model is the point where a material stream leaves the flowsheet.

$$\frac{\mathrm{d}(MU)}{\mathrm{d}t} = \dot{m}_{\mathrm{in}} h_{\mathrm{in}} - \dot{m}_{\mathrm{out}} h_{\mathrm{out}} - \dot{Q} \tag{14}$$

where p_{cavern} is the underground cavern pressure, V is the underground cavern volume, M is the total mass, R is gas constant, T the underground cavern temperature, t is the time, $\dot{m}_{\mathrm{in}}$ is the air mass flow rate into the underground cavern, $\dot{m}_{\mathrm{out}}$ is the air mass flow rate out of the underground cavern, U is the specific internal energy of air, h_{in} is the specific enthalpy of air entering the gas storage cavern, h_{out} is the specific enthalpy of air exiting the gas storage cavern $\dot{Q}$ is the heat transfer rate.

Furthermore, $\dot{Q}$ can be expressed as [29]:

$$\dot{Q} = \alpha A (T - T_{\mathrm{amb}}) \tag{15}$$

where α is the convective heat transfer coefficient between gas storage and environment, A is the surface area of the underground cavern, T_{amb} is the ambient temperature.

Taking Eq. (12), Eq. (13) and Eq. (15) into Eq. (14), the equation can be expressed as:

$$\left(Mc_p - MR\right)\frac{\mathrm{d}T}{\mathrm{d}t} + \dot{m}_{in} c_p (T - T_1) - RT\frac{\mathrm{d}M}{\mathrm{d}t} + \alpha A (T - T_{amb}) = 0 \tag{16}$$

3. CAES system analysis

3.1. System description

gPROMS (general Process Modelling System) is a powerful software platform used for process system modeling and simulation [35–38], enabling engineers and researchers to create detailed mathematical models of complex processes across various industrial sectors [39,40]. It offers flexibility by allowing users to build custom models using a range of modeling paradigms, including continuous and discrete-event modeling [41–43]. gPROMS supports advanced simulations, steady-state calculations, and optimization, facilitating in-depth analysis of process behavior. With extensive libraries of pre-defined models and components, the software accelerates model development and integrates seamlessly with other tools for enhanced functionality and data exchange [44,45].

In Fig. 2, the CAES system is divided into four main parts, including

Table 2
CAES system main parameters.

Serial number	Parameter		Unit	Numerical value
Initial air conditons	Mass flow rate		kg/s	10
	Surroundings temperature		℃	20
	Surroundings pressure		MPa	0.1
Compressor	Compression power(P_c)		/	90 %
	Isentropic efficiency(η_{is})		/	85 %
	Import air pressure(p_1)	Stage 1	MPa	0.099
		Stage 2		0.342
		Stage 3		0.894
		Stage 4		2.344
	Inlet air temperature(T_1)	Stage 1	°C	25
		Stage 2		45
		Stage 3		45
		Stage 4		45
Underground cavern storage	Underground cavern volume (V)		m^3	10^4
	Underground cavern surface area(A)		m^2	$5.12e^3$
	Heat transfer coefficient(α)		W/(m^2·K)	20
	Ambient temperature(T_{amb})		°C	20

the compressor module, heat exchanger module, underground cavern storage module and expander module. Furthermore, gPROMS is used to integrate subsystem modulars.

The compression system includes power input module, a multi-stage compression module, and an inter-stage cooling module. The underground energy storage model adopts the gas tank model, which can calculate the dynamic mass, pressure and temperature inside the cavity. The expansion system includes a flow pressure control module, a multi-stage expansion module, and an inter-stage heating module. The model symbol is given in Table 1.

3.2. System analysis

In this paper, the compressor unit adopts 4-stage compression, and the combination of inter-stage heat transfer. The basic design parameters of the system are given in Table 2.

3.2.1. Parametric analysis of compressor model

In a CAES system, the operational characteristics of compressors serve as core determinants of overall system performance. In order to explore the dynamic operation of the compressor module, the sensitivity analysis of pressure ratio and compression powder subjected to mass flow rate is interrogated in Fig. 3 to Fig. 7. In Fig. 3, the relationship between the pressure ratio and mass flow rate exhibits a clear upward trend. The pressure ratio increases from slightly above 1 to approximately 2.2 as the mass flow rate rises. In Fig. 4, the relationship between pressure increment and mass flow rate further reinforces this pattern. The pressure increment starts near 0 kPa and gradually increases to approximately 110 kPa as the mass flow rate rises. This indicates that at lower mass flow rates, the pressure boost generated by the compressor is relatively small. However, as the mass flow rate increases, the compressor must consume more energy to compress the gas, leading to a significant rise in the pressure ratio. This trend reflects the compressor's compression capacity under different flow conditions, demonstrating a direct positive correlation between performance and mass flow rate.

In Fig. 5, the relationship between compression power and mass flow rate clearly illustrates the energy consumption characteristics of the compressor. Compression power starts near 0 kJ/s and rises steadily to around 4000 kJ/s as the mass flow rate increases. This indicates that at low mass flow rates, the compressor operates with relatively low energy consumption. However, as the flow rate grows, the compressor requires significantly more energy to complete the compression process, resulting in a substantial increase in power consumption.

Overall, the trends observed in these three plots are interrelated, collectively revealing the operational characteristics of the compressor in a CAES system. The pressure ratio, pressure increment, and compression power all increase with rising mass flow rates, reflecting the compressor's performance variations under different operating conditions. In practical applications, it is essential to consider the influence of mass flow rate on compressor operating parameters to optimize compressor design and control strategies, ultimately enhancing overall system efficiency and performance.

Fig. 6 illustrates the variation of gas mass flow rate with pressure ratio and compression power under different CAES operating conditions. The distribution of the contour lines indicates that, at a constant compression power, an increase in the pressure ratio leads to a higher gas mass flow rate. This is because a greater pressure difference drives a

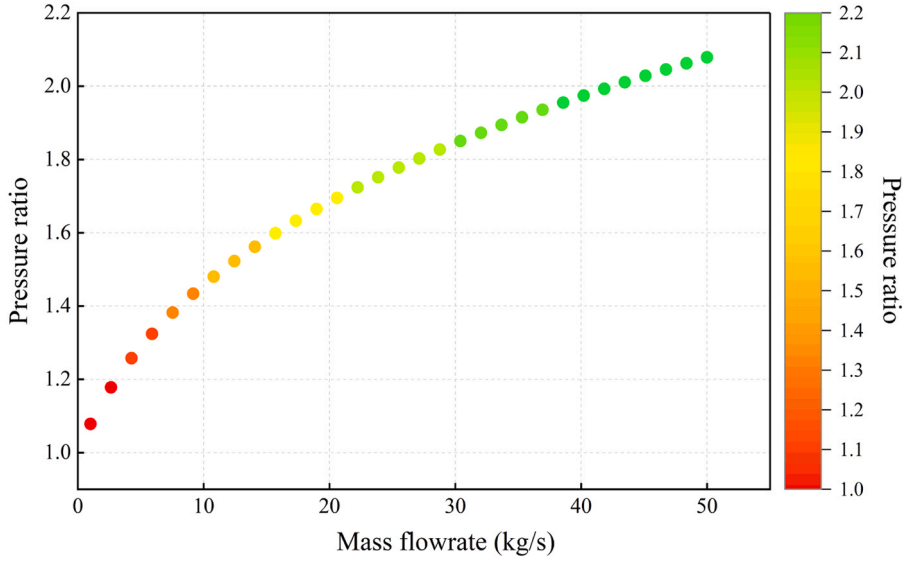

Fig. 3. The relationship between pressure ratio and mass flowrate.

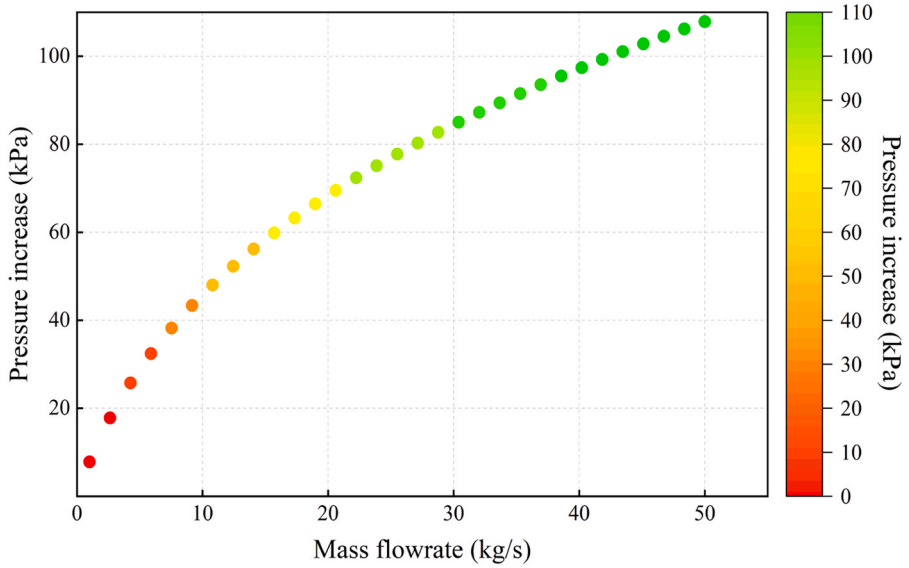

Fig. 4. The relationship between pressure increase and mass flowrate.

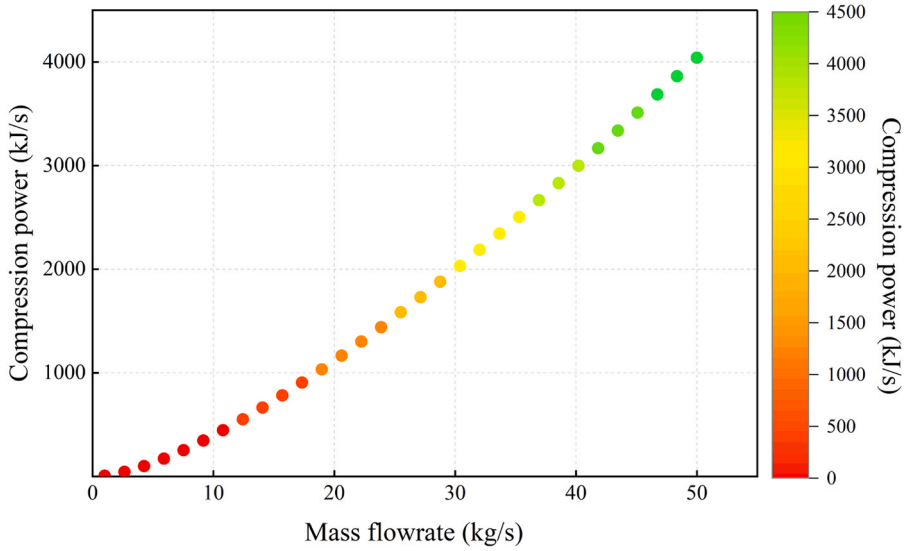

Fig. 5. The relationship between compression power and mass flowrate.

larger mass flow. Similarly, Fig. 7 depicts the relationship between gas mass flow rate, pressure increment, and compression power under various CAES operating conditions. The contour distribution in this figure exhibits a similar pattern to that in Fig. 6. At a given compression power, an increase in pressure increment results in a higher gas mass flow rate. During the gas injection process, variations in the pressure ratio directly affect the pressure and temperature within the storage chamber.

3.2.2. *Parametric analysis of cooler model*

To investigate the dynamic operation of the cooler module, a sensitivity analysis of energy rate and pressure with respect to mass flow rate is conducted, as presented in Fig. 8 to Fig. 11. Fig. 8 demonstrates a pronounced positive correlation between the thermal energy input rate at the cooler inlet and the mass flow rate. The data reveal that lower mass flow rates correspond to diminished energy transfer rates within the cooling system, whereas systematic increases in mass flow rate induce a proportional escalation in thermal power transmission. This relationship highlights distinct thermal loading behaviors across flow regimes, confirming a direct interdependence between mass transport kinetics and heat dissipation efficacy.

In contrast, Fig. 9 exhibits an inverse trend, with the cooler outlet energy rate displaying a progressive reduction and acquiring increasingly negative magnitudes as mass flow rate rises. This behavior originates from amplified thermodynamic interactions at elevated flow rates, where heightened thermal loads intensify energy extraction processes, thereby magnifying negative energy rate values. The observed inverse correlation corresponds to fundamental energy conservation principles governing the cooler's energy balance under variable operational conditions.

Collectively, these complementary trends in Fig. 8 and Fig. 9 delineate the thermodynamic duality of the cooler in CAES systems. The divergent energy rate profiles at inlet and outlet nodes underscore the necessity of accounting for mass flow rate dependencies in both thermal input and output phases. Strategic optimization of cooler geometry and operational protocols, informed by these coupled energy-mass flux relationships, may significantly enhance CAES efficiency and stability under dynamic working conditions.

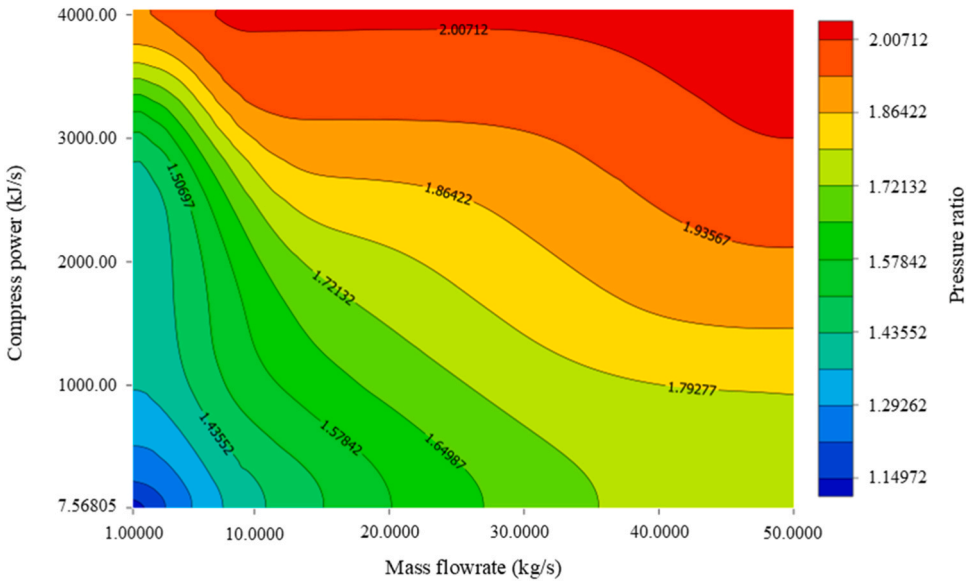

Fig. 6. Variation of compress power and pressure increase subject to mass flowrate.

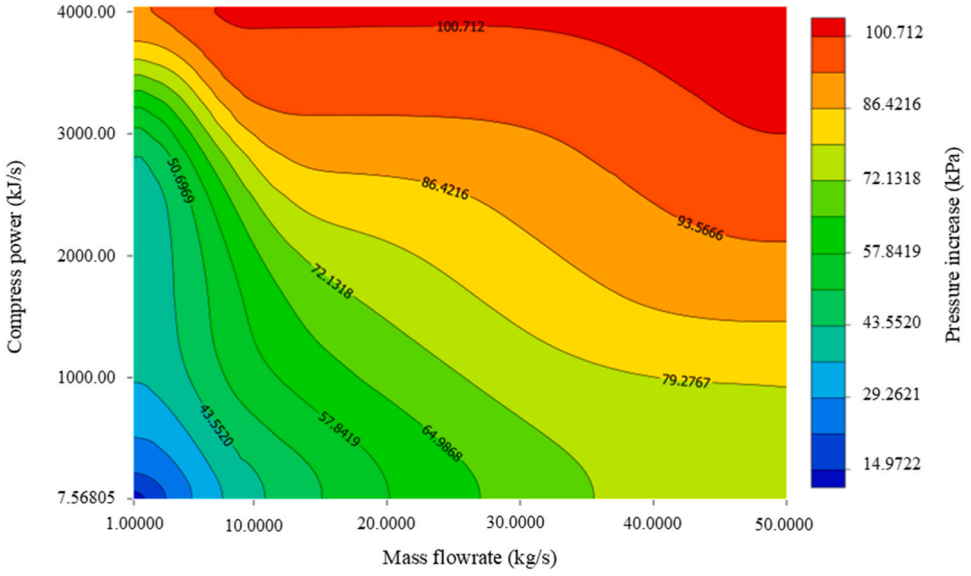

Fig. 7. Variation of compress power and pressure ratio subject to mass flowrate.

Fig. 10 demonstrates coupled dependencies among mass flow rate, inlet temperature, and outlet pressure, revealing monotonic increases in flow rate with both temperature and pressure elevation. This trend adheres to gas dynamic fundamentals: elevated inlet temperatures enhance gas molecular kinetic energy, inducing volumetric expansion that necessitates increased flow rates to maintain constant-pressure conditions. Concurrently, heightened outlet pressure amplifies the system's pressure differential, driving augmented mass flux through the heat exchange geometry. Fig. 11 exhibits countervailing energy rate trends between cooler inlet and outlet nodes under mass flow modulation. Increasing flow rates produce incremental rises in outlet energy rates accompanied by corresponding inlet energy attenuation. The contour gradient density illustrates nonlinear energy transfer dynamics, with steeper rate variations in low-flow regimes transitioning to asymptotic stabilization at higher fluxes. These complementary diagrams collectively delineate the heat exchanger's dual role in CAES operation. Fig. 10 quantifies fluid dynamic constraints while Fig. 11 characterizes thermal energy redistribution limits. The observed parameter interdependencies necessitate holistic consideration of inlet thermal states, pressure differentials, and flow kinematics during system optimization. Strategic redesign of heat exchange geometries and operational protocols, informed by these coupled thermofluidic relationships, could substantially improve CAES energy density and cyclic stability.

3.2.3. Parametric analysis of cavern model analysis

Analysis of Fig. 12 to Fig. 15 provides detailed insights into the thermodynamic behavior of these caverns under varying mass flow rates. Fig. 12 illustrates the relationship between heat dissipation and mass flow rate, revealing a marked increase in heat loss as flow rate rises. At low mass flow rates (<10 kg/s), heat dissipation increases gradually, then exhibits a steady rise before stabilizing at higher flow rates (>40 kg/s). This trend suggests limited thermal exchange between the cavern and its surroundings at lower flows, with enhanced convective heat transfer prevailing at higher flows. For example, heat dissipation is approximately 0.5 kJ/s at 1 kg/s, increasing to 2.5 kJ/s at 50 kg/s.

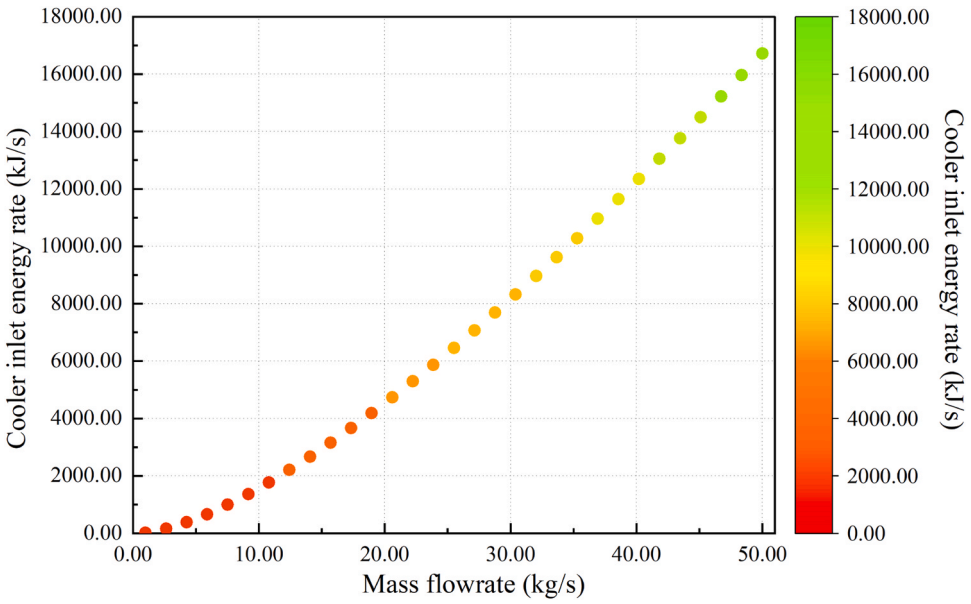

Fig. 8. The relationship between cooler inlet energy rate and mass flowrate.

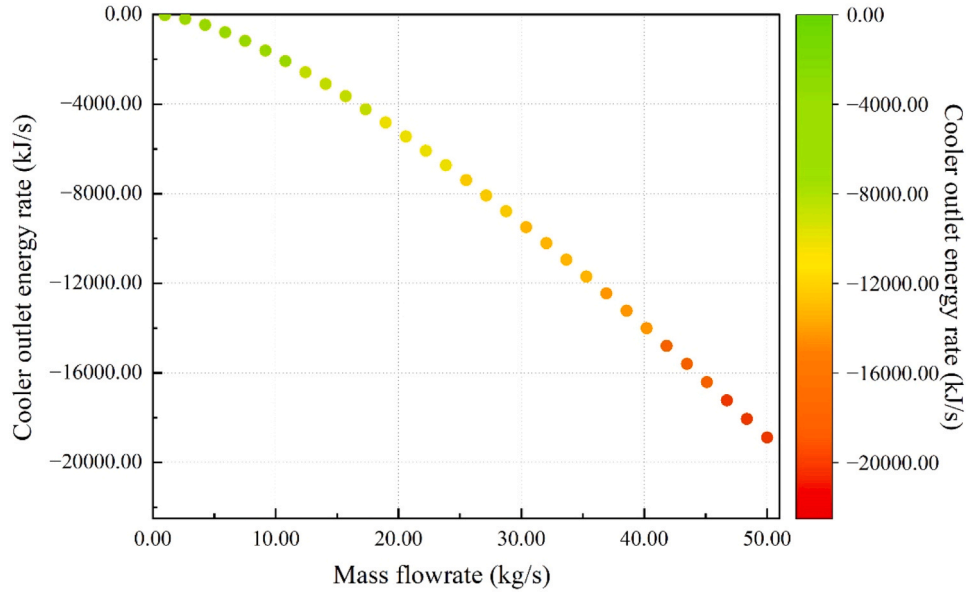

Fig. 9. The relationship between cooler outlet energy rate and mass flowrate.

Fig. 13 depicts the correlation between temperature and mass flow rate, showing a consistent temperature increase with rising flow. At low flow rates, the temperature rises sharply, then increases more gradually, eventually plateauing at elevated flow rates. This pattern confirms a direct positive relationship between temperature and mass flow rate, with representative values of 40°C at 1 kg/s and 140°C at 50 kg/s. These observed trends are closely tied to the heat transfer mechanisms within the cavern. At low flow rates, slow gas movement limits heat exchange to conduction and natural convection. As flow rate increases, accelerated gas motion enhances forced convection, amplifying heat transfer and resulting in greater heat dissipation and temperature elevation. The stabilization at high flow rates indicates that the cavern's heat exchange capacity reaches saturation.

Collectively, these findings clarify the thermodynamic behavior of caverns in CAES systems. Both heat dissipation and temperature display flow-dependent increases, reflecting distinct operational transitions across flow regimes. These insights emphasize the need for thorough optimization of cavern design and operational strategies, particularly in managing flow parameters, to improve the overall efficiency and stability of CAES systems.

In the analysis of cavern operational characteristics in CAES systems, two data figures reveal dynamic correlations between critical parameters from distinct perspectives. In Fig. 14, plotted with mass flow rate on the horizontal axis and temperature on the vertical axis, employs pressure contours to illustrate the synergistic variation of these three parameters. As mass flow rate increases, air temperature rises markedly, accompanied by a pronounced upward clustering of pressure contours. This phenomenon stems from the continuous operation of compressors during the energy storage phase: as more air is compressed into the cavern, molecular kinetic energy converts to thermal energy via intense friction and collisions, elevating temperature. Simultaneously, forced compression within the confined space directly amplifies system

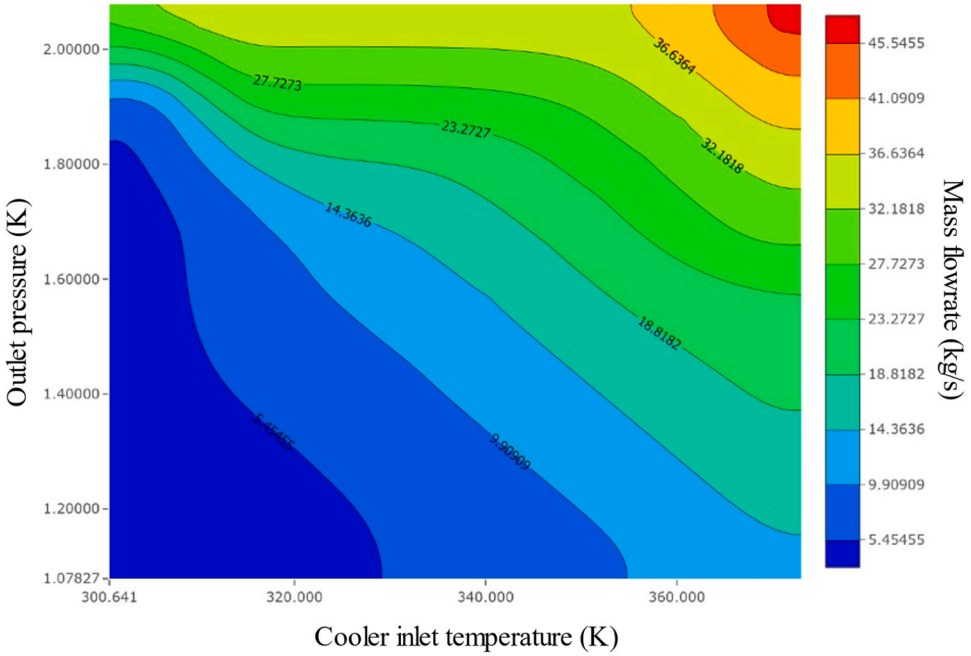

Fig. 10. Variation of cooler inlet temperature and outlet pressure subject to mass flowrate.

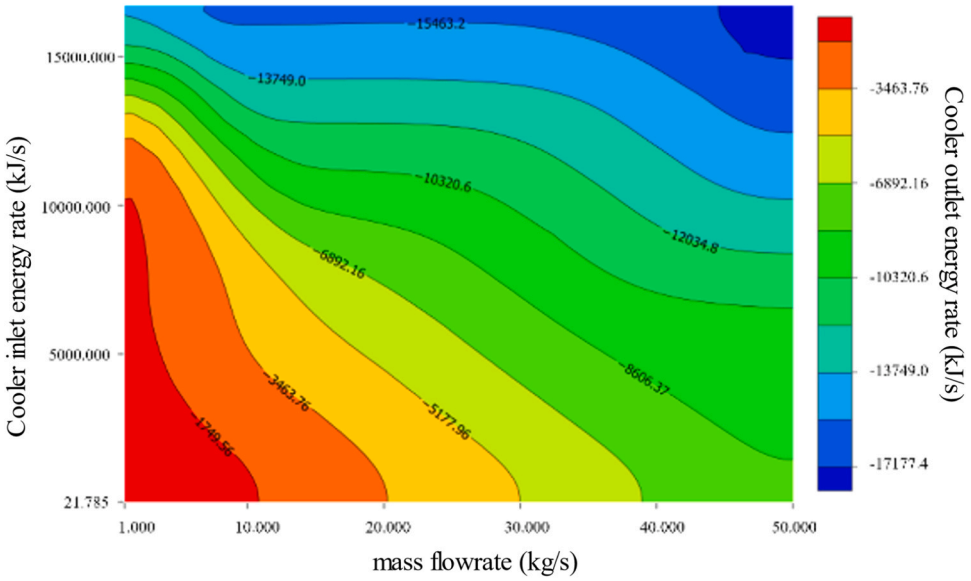

Fig. 11. Variation of cooler inlet energy rate and cooler outlet energy rate subject to mass flowrate.

pressure. The observed positive correlation between pressure and temperature validates the applicability of the ideal gas law while highlighting the critical influence of compressor power on energy storage density.

Fig. 15 focuses on the coupling between mass flow rate and heat loss, integrating pressure contours to elucidate thermodynamic dissipation mechanisms in real-world systems. Despite theoretical adherence to adiabatic assumptions during compression, data reveal near-linear growth in heat loss with increasing mass flow rate, alongside rising pressure. This arises from multiphysics coupling in engineering practice: during high-speed compressor operation, expanded contact areas between air, mechanical components, and cavern walls enhance convective heat transfer. Additionally, elevated thermal conductivity of compressed gas under high-pressure conditions exacerbates heat dissipation to the surroundings. Notably, while pressure increase correlates positively with mass flow rate, its growth rate diminishes at higher flows, potentially indicating declining compression efficiency under cavern volume constraints.

Comprehensive analysis demonstrates that mass flow rate, as a core control variable in CAES systems, not only directly governs energy storage density (via pressure elevation) but also triggers significant thermodynamic effects. Fig. 14 quantifies temperature-pressure co-evolution patterns critical for thermal management, while Fig. 15 exposes heat loss mechanisms that underscore the urgency of optimizing adiabatic designs, such as cavern insulation layers and compressor cooling systems. These interconnected principles provide theoretical foundations for balancing storage efficiency and thermal losses, guiding engineers to dynamically adjust flow parameters in operational strategies. Examples include reducing flow rates during high-pressure phases to suppress heat dissipation or implementing staged compression to

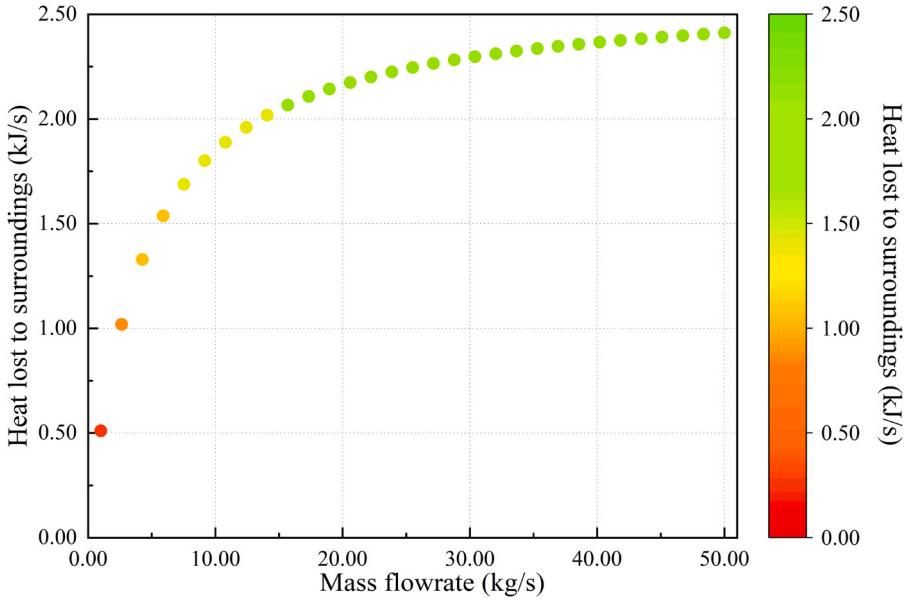

Fig. 12. The relationship between heat lost surroundings and mass flowrate.

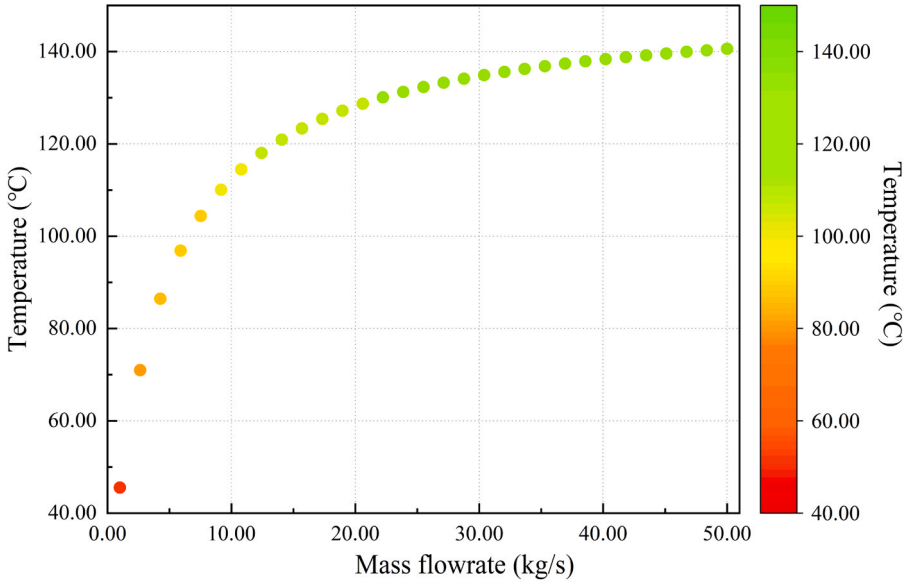

Fig. 13. The relationship between temperature and mass flowrate.

control temperature rise rates, ultimately achieving synergistic optimization of system energy efficiency and equipment longevity.

4. Discussions

A comprehensive CAES process system model was established through the gPROMS platform demonstrating significant advancements in addressing critical gaps identified in prior research. In contrast to previous studies predominantly focusing on isolated subsystem analyses [25–27], our integrated approach explicitly connects compressor, heat exchanger, underground cavern storage, and expander modules through inlet-outlet equilibrium constraints, thereby enabling holistic simulations of dynamic interactions. This capability is notably absent in earlier works such as Hossein et al.'s decentralized configuration [25] and Lv et al.'s parameter optimization framework [26]. This integration aligns with Sciacovelli et al.'s emphasis on transient behavior analysis [27] but extends its scope by incorporating bidirectional thermodynamic coupling between surface and subsurface components, a feature essential for capturing real-world operational interdependencies.

The implications of this work are twofold. First, the model provides a high-fidelity framework for evaluating cavern injection characteristics under variable mass flow rates, as a critical advancement given the scarcity of integrated thermodynamic analyses in existing CAES literature [19–21]. The revealed nonlinear relationships between flow rates, pressure ratios, and compression power offer actionable insights for optimizing compressor staging and thermal management strategies. Second, by bridging the long-standing disconnect between overground and underground subsystems, the study establishes a methodological foundation for assessing system level efficiency trade-offs, particularly in hybrid CAES configurations integrating renewable generation.

However, several limitations warrant consideration. While the model successfully captures injection-phase dynamics, its exclusion of energy recovery mechanisms, specifically expander hysteresis effects and waste heat utilization, makes it challenging to conduct

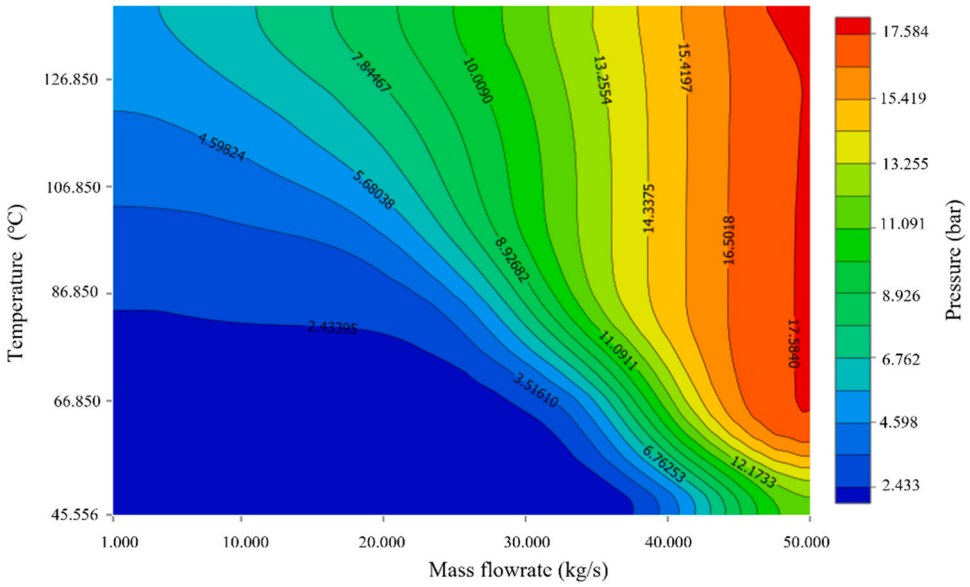

Fig. 14. Variation of cavern temperature and pressure subject to mass flowrate.

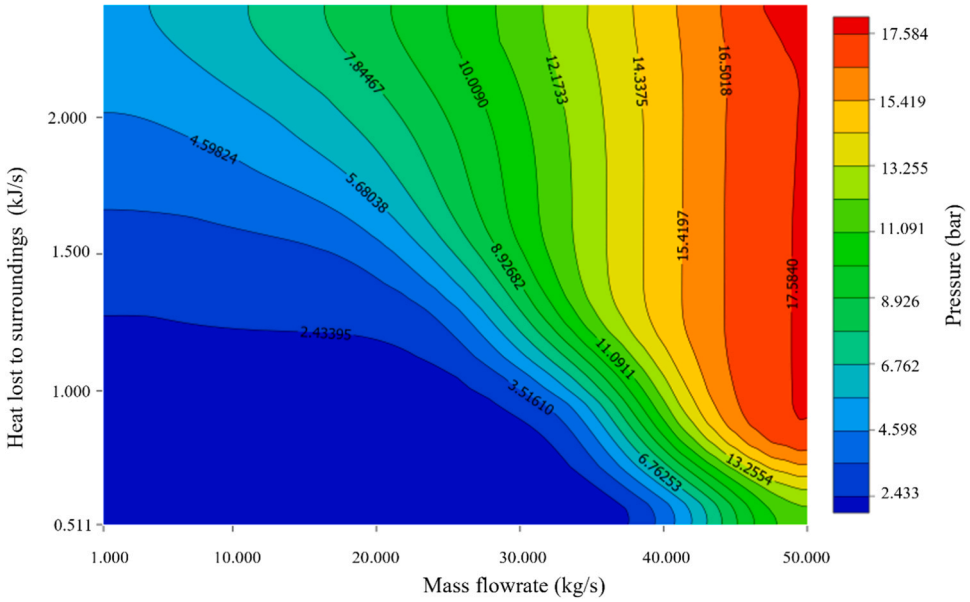

Fig. 15. Variation of heat lost to surroundings and cavern pressure subject to mass flowrate.

comprehensive efficiency evaluations comparable to those in Arabkoohsar et al.'s advanced adiabatic CAES analyses. [30]. Furthermore, the assumption of ideal gas behavior and negligible pipeline pressure drops (Section 2) may underestimate real-world thermal losses, particularly in large-scale geological reservoirs where non-ideal gas effects become pronounced. Additionally, the current validation relies solely on theoretical simulations, lacking experimental corroboration against operational CAES facilities like the Huntorf plant [19].

To address these limitations and extend the research scope, the strategic directions emerge for future work. First, integrating transient expander performance models with the existing framework would enable full charge-discharge cycle analyses, particularly critical for evaluating pressure-temperature hysteresis impacts on turbine efficiency. This integration aims to quantitatively evaluate critical system interactions, particularly the thermodynamic trade-offs inherent in compressor-expander matching strategies, thermal buffering mechanisms, and overall energy conversion efficiency throughout charge-discharge cycles. Second, experimental validation through scaled cavern prototypes or operational data from existing salt dome facilities could refine heat transfer coefficients and verify the model's predictive accuracy under non-ideal conditions.

5. Conclusion

Compressed Air Energy Storage (CAES) presents a compelling solution for mitigating the intermittency of renewable energy sources like solar and wind. This study establishes a comprehensive thermodynamic model of the CAES system interlinking its individual components using the gPROMS platform. The integrated components, featured with the physical soundness, allow for a detailed analysis of the overall performance and dynamic interactions of large-scale CAES system. By connecting both overground and underground subsystems, the model facilitates a thorough examination of gas injection behaviors within the underground cavern. It reveals crucial dynamic changes in temperature,

pressure, and mass flow rate during the injection phase. The temperature and pressure experience rapid increases at the start of injection before stabilizing as equilibrium is reached. The established system model addresses the long-standing disconnections between overground and underground systems, providing scientific insights into gas dynamics under diverse operating conditions.

The study also uncovers vital relationships among key parameters, including a positive correlation between mass flow rate and pressure ratio, as well as a significant nonlinear increase in compression power with increasing mass flow rate. Additionally, the cooler outlet energy rate exhibits a progressive decline, becoming increasingly negative as the mass flow rate rises. These findings provide improved understanding of the CAES system performance from holistic perspective. Further attempts of model validation and energy efficiency should be conducted to extend the research scope. This study opens new avenues for optimizing and enhancing the performance of CAES systems, ultimately supporting the transition to a more sustainable energy ecosystem.

Funding

National Natural Science Foundation of China Excellent Young Scientists Fund Program, Deep Earth Probe and Mineral Resources Exploration-National Science and Technology Major Project (grant No. 2024ZD1004105), Shandong Excellent Young Scientists Fund Program (Overseas) (grant No. 2022HWYQ-020), Shenzhen Science and Technology Program (grant No. JCYJ20220530141016036, GJHZ20240218113359001).

CRediT authorship contribution statement

LiGe Wang: Investigation, Methodology, Writing – original draft. **Cunzhuang Lu, Shishu Zhang and Di Peng:** Methodology, Writing – review & editing. **Qingrong Xiong and Xizhong Chen:** Supervision, Writing – review & editing. **Hongling Ma and Zizheng Sun:** Methodology. **Liping Li:** Funding acquisition, Investigation, Methodology.

Declaration of Competing Interest

The authors declare that they have no known competing financial interests or personal relationships that could have appeared to influence the work reported in this paper.

Acknowledgements

The authors gratefully acknowledge to Beijing Hegong Simulation Technology Company Limited for provision of gPROMS license. We gratefully acknowledge Dr. Ming Gong and Dr. Hualiang Zhao for their helpful process system modelling. This work was supported by National Natural Science Foundation of China Excellent Young Scientists Fund Program, Deep Earth Probe and Mineral Resources Exploration-National Science and Technology Major Project (grant No. 2024ZD1004105), Shandong Excellent Young Scientists Fund Program (Overseas) (grant No. 2022HWYQ-020), Shenzhen Science and Technology Program (grant No. JCYJ20220530141016036, GJHZ20240218113359001).

References

[1] B.R. Hou, S.T. Shangguan, Y.H. Niu, et al., Unique properties of rock salt and application of salt caverns on underground energy storage: a mini review, Energy Sources, Part A: Recovery, Util., Environ. Eff. 46 (1) (2024) 621–635.
[2] X.Y. Chen, Y. Chen, L. Fu, et al., Photovoltaic-driven liquid air energy storage system for combined cooling, heating and power towards zero-energy buildings, Energy Convers. Manag. 300 (2024) 117959.
[3] N. Apergis, N. Carmona-González, L.A. Gil-Alana, Persistence in silver prices and the influence of solar energy, Resour. Policy 69 (2020) 101857.
[4] S.K. Qin, C.C. Xia, S.W. Zhou, Air tightness of compressed air storage energy caverns with polymer sealing layer subjected to various air pressures, J. Rock. Mech. Geotech. Eng. 15 (8) (2023) 2105–2116.
[5] C. Gao, Performance investigation of solar-assisted supercritical compressed carbon dioxide energy storage systems, J. Energy Storage 79 (2024) 110179.
[6] J.Y. Fang, H.L. Ma, C.H. Yang, et al., Airtightness evaluation of lined caverns for compressed air energy storage under thermo-hydro-mechanical (THM) coupling, Energy 308 (2024) 132996.
[7] F. Wan, Z.M. Jiang, X. Tian, et al., A thermo-hydro-mechanical damage model for lined rock cavern for compressed air energy storage, J. Energy Storage 78 (2024) 110186.
[8] R.Y. Cao, W.Q. Li, X.W. Cong, et al., Energy, exergy and economic (3E) analysis and multi-objective optimization of a combined cycle power system integrating compressed air energy storage and high-temperature thermal energy storage, Appl. Therm. Eng. 238 (2024) 122077.
[9] I.K. Iliev, A.V. Fedyukhin, D.V. Semin, et al., Prospects of hydrogen application as a fuel for large-scale compressed-air energy storages, Energies 17 (2) (2024) 518.
[10] F.S. Koohi, M.A. Rosen, A review of energy storage types, applications and recent developments, J. Energy Storage 27 (2020) 101047.
[11] A.G. Olabi, T. Wilberforce, M.A. Abdelkareem, et al., Critical review of flywheel energy storage system, Energies 14 (8) (2021) 2159.
[12] D. Fernandes, F. Pitié, G. Cáceres, et al., Thermal energy storage: how previous findings determine current research priorities, Energy 39 (1) (2012) 246–257.
[13] W.Y. Fu, W.Q. Sun, X.Y. Huo, Design and thermodynamic investigation of a waste heat-assisted compressed air energy storage system integrating thermal energy storage and organic rankine cycle, Energy Technol. 12 (2) (2024) 2300838.
[14] Y.R. Liang, P. Li, L.L. Xing, et al., Current status of thermodynamic electricity storage: principle, structure, storage device and demonstration, J. Energy Storage 80 (2024) 110347.
[15] H.M. Kim, J. Rutqvist, D.W. Ryu, et al., Exploring the concept of compressed air energy storage (CAES) in lined rock caverns at shallow depth: a modeling study of air tightness and energy balance, Appl. Energy 92 (2012) 653–667.
[16] R. Kumar, D.H. Lee, Ü. Ağbulut, et al., Different energy storage techniques: recent advancements, applications, limitations, and efficient utilization of sustainable energy, J. Therm. Anal. Calorim. (2024).
[17] Y. Ma, Q.H. Rao, D.Y. Huang, et al., A new theoretical model of local air-leakage seepage field for the compressed air energy storage lined cavern, J. Energy Storage 49 (2022) 104160.
[18] X.Y. Zhuang, R.Q. Huang, C. Liang, et al., A coupled thermo-hydro-mechanical model of jointed hard rock for compressed air energy storage, Math. Probl. Eng. 2014 (2014) 179169.
[19] L. Szablowski, T. Morosuk, Advanced exergy analysis of adiabatic underwater compressed air energy storage system, Entropy 25 (1) (2023) 77.
[20] X.J. Zhang, Y. Li, Z.Y. Gao, et al., Overview of dynamic operation strategies for advanced compressed air energy storage, J. Energy Storage 66 (2023) 107408.
[21] T.M.I. Mahlia, T.J. Saktisahdan, A. Jannifar, et al., A review of available methods and development on energy storage; technology update, Renew. Sust. Energy Rev. 33 (2014) 532–545.
[22] E. Bazdar, M. Sameti, F. Nasiri, et al., Compressed air energy storage in integrated energy systems: a review, Renew. Sustain. Energy Rev. 167 (2022) 112701.
[23] G. Dib, P. Haberschill, R. Rullière, et al., Thermodynamic investigation of quasi-isothermal air compression/expansion for energy storage, Energy Convers. Manag. 235 (2021) 114027.
[24] O. Burian, P. Dančová, Compressed air energy storage (CAES) and liquid air energy storage (LAES) technologies-a comparison review of technology possibilities, Processes 11 (11) (2023) 3061.
[25] H. Safaei, D.W. Keith, Compressed air energy storage with waste heat export: an alberta case study, Energy Convers. Manag. 78 (2014) 114–124.
[26] S. Lv, W. He, A.F. Zhang, et al., Modelling and analysis of a novel compressed air energy storage system for trigeneration based on electrical energy peak load shifting, Energy Convers. Manag. 135 (2017) 394–401.
[27] A. Sciacovelli, Y.L. Li, H.S. Chen, et al., Dynamic simulation of adiabatic compressed air energy storage (A-CAES) plant with integrated thermal storage-link between components performance and plant performance, Appl. Energy 185 (2017) 16–28.
[28] Q. He, G.Q. Li, C. Lu, et al., A compressed air energy storage system with variable pressure ratio and its operation control, Energy 169 (2019) 881–894.
[29] H. Jin, P. Liu, Z. Li, Dynamic modeling and design of a hybrid compressed air energy storage and wind turbine system for wind power fluctuation reduction, Comput. Chem. Eng. 122 (2019) 59–65.
[30] A. Arabkoohsar, H.R. Rahrabi, A.S. Alsagri, et al., Impact of off-design operation on the effectiveness of a low-temperature compressed air energy storage system, Energy 197 (2020) 117176.
[31] J. Chen, D. Jiang, W. Liu, et al., Research progress of solution mining and comprehensive utilization of salt cavern, Bull. Natl. Nat. Sci. Found. China 35 (6) (2021) 911–916.
[32] Y. Li, Y. Li, Y. Liu, et al., Compressed air energy storage in aquifers: basic principles, considerable factors, and improvement approaches, Rev. Chem. Eng. 37 (5) (2019) 561–584.
[33] J. Wan, Y. Sun, Y. He, et al., Development and technology status of energy storage in depleted gas reservoirs, Int. J. Coal Sci. Technol. 11 (1) (2024) 29.
[34] Z.C. Wang, J.X. Li, X.J. Xue, et al., A review of several issues for compressed gas energy storagein lined rock cavern, Hazard Control Tunn. Undergr. Eng. 6 (1) (2024) 1–13 (in Chinese).
[35] R. Leeming, T. Mahmud, K.J. Roberts, et al., Development of a digital twin for the prediction and control of supersaturation during batch cooling crystallization, Ind. Eng. Chem. Res. 62 (28) (2023) 11067–11081.

[36] H. Qayyum, I.I. Cheema, M. Abdullah, et al., One-dimensional modeling of heterogeneous catalytic chemical looping steam methane reforming in an adiabatic packed bed reactor, Front. Chem. 11 (2023) 1295455.
[37] R. Garma, D. Sioud, H. Binous, et al., Introduction to the modeling of complex chemical reaction equilibrium using gPROMS® and GAMS®, Comput. Appl. Eng. Educ. 32 (3) (2024).
[38] G. Tian, A. Koolivand, Z.Y. Gu, et al., Development of an RTD-based flowsheet modeling framework for the assessment of in-process control strategies, AAPS PharmSciTech 22 (1) (2021) 25.
[39] L.G. Wang, S.U. Pradhan, C. Wassgren, et al., A breakage kernel for use in population balance modelling of twin screw granulation, Powder Technol. 363 (2020) 525–540.
[40] I. Naşcu, N.A. Diangelakis, S.G. Muñoz, et al., Advanced model predictive control strategies for evaporation processes in the pharmaceutical industries, Comput. Chem. Eng. 173 (2023) 108212.
[41] L.G. Wang, J.P. Morrissey, D. Barrasso, et al., Model driven design for twin screw granulation using mechanistic-based population balance model, Int. J. Pharm. 607 (2021) 120939.
[42] J.H. Chang, G.H. Lee, D. Adams, et al., Multiscale modeling and integration of a combined cycle power plant and a two-tank thermal energy storage system with gPROMS and SimCentral, Korean J. Chem. Eng. 38 (7) (2021) 1333–1347.
[43] D.M. Aliaga, C.P. Romero, R. Feick, et al., Modelling, simulation, and optimisation of a novel liquid piston system for energy recovery, Appl. Energy 357 (2024) 122506.
[44] L.G. Wang, R.H. Ge, X.Z. Chen, et al., Multiscale digital twin for particle breakage in milling: from nanoindentation to population balance model, Powder Technol. 386 (2021) 247–261.
[45] Z.P. Li, L.G. Wang, W.Z. Chen, et al., Scale-up procedure of parameter estimation in selection and breakage functions for impact pin milling, Adv. Powder Technol. 31 (8) (2020) 3507–3520.

Liping Li, professor, doctoral supervisor, and a recipient of the National Outstanding Youth Fund at School of Qilu Transportation of Shandong University. He has been honored with several prestigious awards, including the Chinese Youth Science and Technology Award, the Tianyou Zhan Achievement Award, and the Tencent Scientific Exploration Award. In addition, he has also received 1 second-class National Science and Technology Progress Award and 1 second-class National Technical Invention Award, as well as 3 first-class provincial and ministerial-level Science and Technology Progress Awards and Technical Invention Awards (1st position). His primary research area is focused on intelligent construction in underground engineering and disaster prevention and control. He has an H-index of 44, with over 90 SCI/EI papers published as the first author or corresponding author. Among them, 1 paper has been listed among the "China Top 100", 6 papers have received high citations, and ranked in the top 2 % of the world's top scientists. Additionally, he holds two USA patents and 7 international patents under the Patent Cooperation Treaty (PCT), as well as 57 Chinese invention patents and 14 software copyrights (all as the first author). Moreover, he has been actively involved in the compilation of 19 standards and engineering methods.